Tapered GRIN fiber microsensor

Felipe Beltrán-Mejía,[1,2] **Claudecir R. Biazoli**[1] **and Cristiano M. B. Cordeiro**[1,*]

[1] *All authors are with the Instituto de Física "Gleb Wataghin", Universidade Estadual de Campinas – UNICAMP, Campinas, SP, Brazil*

[2] *Presently at National Institute of Telecommunications (INATEL), Santa Rita do Sapucaí, MG, Brazil*

**cmbc@ifi.unicamp.br*

Abstract: The sensitivity of an optical fiber microsensor based on inter-modal interference can be considerably improved by tapering a short extension of the multimode fiber. In the case of Graded Index fibers with a parabolic refractive index profile, a meridional ray exhibits a sinusoidal path. When these fibers are tapered, the period of the propagated beam decrease down-taper and increase up-taper. We take advantage of this modulation –along with the enhanced overlap between the evanescent field and the external medium– to substantially increase the sensitivity of these devices by tuning the sensor's maximum sensitivity wavelength. Moreover, the extension of this device is reduced by one order of magnitude, making it more propitious for reduced space applications. Numerical and experimental results demonstrate the success and feasibility of this approach.

OCIS codes: (230.0230) Optical devices; (060.2370) Fiber optics sensors.

References and links

1. H. Y. Tam, S. Y. Liu, B. O. Guan, W. H. Chung, T. H. Chan, and L. K. Cheng, "Fiber bragg grating sensors for structural and railway applications," in "Advanced Sensor Systems and Applications II," 5634, 85–97 (2005).
2. J. Villatoro, D. Monzón-Hernández, and E. Mejía, "Fabrication and modeling of uniform-waist single-mode tapered optical fiber sensors," Appl. Opt. **42**, 2278–2283 (2003).
3. A. Kumar, R. K. Varshney, S. A. C, and P. Sharma, "Transmission characteristics of SMS fiber optic sensor structures," Optics Communications **219**, 215 – 219 (2003).
4. S. M. Tripathi, A. Kumar, R. K. Varshney, Y. P. Kumar, E. Marin, and J.-P. Meunier, "Strain and temperature sensing characteristics of single-mode–multimode–single-mode structures," J. Lightwave Technol. **27**, 2348–2356 (2009).
5. C. R. Biazoli, S. Silva, M. A. R. Franco, O. Frazão, and C. M. B. Cordeiro, "Multimode interference tapered fiber refractive index sensors," Appl. Opt. **51**, 5941–5945 (2012).
6. F. Beltrán-Mejía, J. H. Osório, C. R. Biazoli, and C. M. B. Cordeiro, "D-microfibers," J. Lightwave Technol. **31**, 2756–2761 (2013).
7. P. Wang, G. Brambilla, M. Ding, Y. Semenova, Q. Wu, and G. Farrell, "Investigation of single-mode–multimode–single-mode and single-mode–tapered-multimode–single-mode fiber structures and their application for refractive index sensing," J. Opt. Soc. Am. B **28**, 1180–1186 (2011).
8. R. S. Pillai, D. Lorenser, and D. D. Sampson, "Deep-tissue access with confocal fluorescence microendoscopy through hypodermic needles," Opt. Express **19**, 7213–7221 (2011).
9. Y. Liu and L. Wei, "Low-cost high-sensitivity strain and temperature sensing using graded-index multimode fibers," Appl. Opt. **46**, 2516–2519 (2007).
10. *Comsol Multiphysics*, Burlington, MA, USA (2014). Version 4.4.
11. A. Ghatak and K. Thyagarajan, *An Introduction to Fiber Optics* (Cambridge University Press, 1998), chap. 9.
12. K. Shiraishi and S.-I. Kuroo, "A new lensed-fiber configuration employing cascaded GI-fiber chips," J. Lightwave Technol. **18**, 787 (2000).
13. R. D. Guenther, *Modern Optics* (Wiley, 1990), chap. 5.

#221963 - $15.00 USD Received 29 Aug 2014; revised 10 Nov 2014; accepted 10 Nov 2014; published 1 Dec 2014

14. H. Kogelnik, "On the propagation of gaussian beams of light through lenslike media including those with a loss or gain variation," Appl. Opt **4**, 1562–1569 (1965).
15. T. Birks and Y. Li, "The shape of fiber tapers," J. Lightwave Technol. **10**, 432–438 (1992).

1. Introduction

In the last decade, optical fiber sensors have been a subject of intense research and development due to their well-know advantages such as high resolution, low-cost, ease of construction and immunity to electromagnetic radiation. A growing trend towards new designs that improves the accuracy and versatility of these sensors is revealed by the myriad of applications now used in industry, civil engineering [1], and as support to other research fields such as medicine and biology. As stated by [2], most of the optical fiber sensors can be classified into two categories: grating-based fiber devices [1] and evanescent field fiber sensors [2–6]. The former are devices with periodic disturbances recorded at the core's refractive index – Bragg or Long Period Gratings – that reflect or transmit part of the input spectrum depending on the periodicity of the core's refractive index. The latter category expose the guided field to the environment – by tapering the fiber or removing the clad– serving as a transducer useful as a sensing instrument.

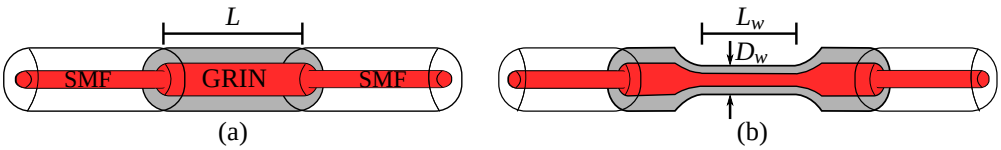

Fig. 1. (a) Scheme of a conventional SMS sensor of length L and (b) a tapered SMS sensor as proposed here, with a waist of length L_w and diameter D_w.

A simplistic and accurate evanescent field fiber sensor can be constructed by splicing a multimode fiber (MMF) in-between two single-mode fibers (SMF) as shown in Fig. 1(a). Such optical devices, known as SMS sensors, are well known for their robustness and ease of use [3–5]. The multiple modes excited at the MMF will interfere creating an output pattern that depends mainly on the phase difference ϕ between the different modes, that is, the difference between the propagation constants $\beta_j - \beta_k$ times the length of the multimode fiber L. When light couples from the input SMF to the MMF, several modes are excited with an associated modal amplitude determined by the overlap integral,

$$a_i = \int \psi_S \psi_i^* \mathrm{d}A \quad ,$$

where ψ_S is the field inside the input single-mode fiber and ψ_i^* is the complex conjugate of the field associated to the ith mode inside the multimode fiber with a cross-section area A. In the same way as in [3, 7], assuming a perfect alignment between the fibers it is only necessary to include axially symmetric linear polarization LP_{0i} modes in our analysis herein.

As shown in [3], when light is coupled at the output SMF fiber, the transmission spectrum will depend basically on the modal amplitudes a_i and the phase difference,

$$P(\lambda) = \left| a_1^2 + a_2^2 e^{j(\beta_1-\beta_2)L} + \cdots + a_i^2 e^{j(\beta_1-\beta_i)L} + \cdots \right|^2 . \tag{1}$$

As a result, the transmission spectrum shows several peaks that are sensitive to any parameter that affects the phase difference between the fundamental mode and the higher order modes, such as strain and temperature.

Usually, SMS sensors are fabricated with a step-index multimode waveguide [5, 7]. Here we

#221963 - $15.00 USD Received 29 Aug 2014; revised 10 Nov 2014; accepted 10 Nov 2014; published 1 Dec 2014

used Graded-Index (GRIN) fibers for the multimode waveguide of the SMS sensor. This type of fibers are well known for reducing modal dispersion and are used in metro telecom networks and high-resolution microendoscopes [8] between other several applications. The reason for choosing GRIN fibers is due to the few modes excitation which simplifies the analysis and –as a consequence of the latter– the output spectrum of the SMS sensor is a well resolved series of peaks compared with those made of step-index multimode fibers [5, 9].

In the following, we develop an analytical approach in order to study the effects of the multimode fiber length at the output spectrum. We study the effects of tapering a GRIN fiber as part of an SMS sensor. This will increase the overlap between the evanescent field and the external material, resulting in an enhanced sensitivity for the external refractive index. Also, as it will be shown below, the spectral region with maximum sensitivity can also be controlled by adjusting the taper waist. At the same time, a better resolved output spectrum was obtained. Below, a brief explanation of the theory behind the tapered SMS sensor is presented followed by the numerical and experimental results. Finally, results and discussion lead towards the concluding remarks.

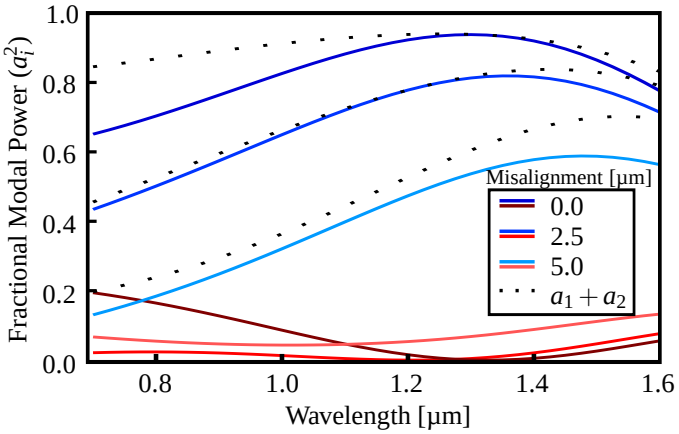

Fig. 2. Numerical results for the fractional modal power of the first two lower order modes using different misalignment values at the splice between the singlemode fiber and the GRIN fiber. As shown in the legend box, bluish and reddish solid lines represent the modal amplitude for LP_{01} and LP_{02} respectively. All results obtained using a Finite Element software [10].

2. Analytic approach

After disregarding all terms other than the first two at the right of Eq. (1), the difference between the propagation constants for the LP_{01} and LP_{02} will determine the intensity output. This assumption is reinforced by the fact that more than 80% of the fractional modal power resides between these two modes as stated by [4] and as shown by the dotted curve at the top of Fig. 2. As it will be shown later, $\beta_1 - \beta_2$ as a function of λ can be approximated as a parabolic function of the type $p + q(\lambda - \lambda_0)^2$, where (p, q) are fitting parameters and λ_0 is the critical wavelength (maximum or minimum of the parabola). After simple algebra, one obtains an expression that relates the Free Spectral Range – the distance between two consecutive peaks, kth and $(k+1)$th, from the output intensity spectrum– with the mean wavelength $\bar{\lambda} = (\lambda_k + \lambda_{k+1})/2$,

$$\mathrm{FSR} \approx \frac{\pi}{qL(\lambda - \lambda_0)}. \tag{2}$$

#221963 - $15.00 USD Received 29 Aug 2014; revised 10 Nov 2014; accepted 10 Nov 2014; published 1 Dec 2014

Values for p, q and λ_0 are obtained after fitting the previous parabolic function with analytic expressions found for the propagation constants in an infinite parabolic index medium [11].

Colored marks in Fig. 3(a) represent experimental measurements for the FSR as a function of wavelength when broadband light was sent through the single-mode fiber and collected in an optical spectrum analyzer using an 82 cm long GRIN fiber GIF625 from Thorlabs with core/cladding diameter of 62.5/125 µm, parabolic profile and maximum refractive index of 1.4858 RIU at $\lambda = 656.2$ nm. To ensure single-modeness inside the SMF fibers, Newport FS-V fibers were used for wavelengths under 0.98 µm and Corning SMF-28 fibers were used over 1.2 µm. All measurements where done at room temperature $T = 20\,^{\circ}$C, fixing the fiber straight while being careful not to stretch the fiber in order to avoid curvature and/or strain effects.

The solid lines in Fig. 3 represent Eq. (2) plotted with the parameters next to each curve. Although the discrepancy is significant, the general trend can be observed by using a simple expression. Once validated, this approach can be used in order to predict the effect of L in the transmission output as shown in Fig. 3(b). This illustrate one of the main motivations behind this work: a conventional SMS sensor requires a multimode fiber with an extension $L > 3$ m in order to have an FSR under 10 nm. Here we explore the effects of tapering the multimode fiber of an SMS sensor in order to enhance the sensitivity and reduce the extension of these devices.

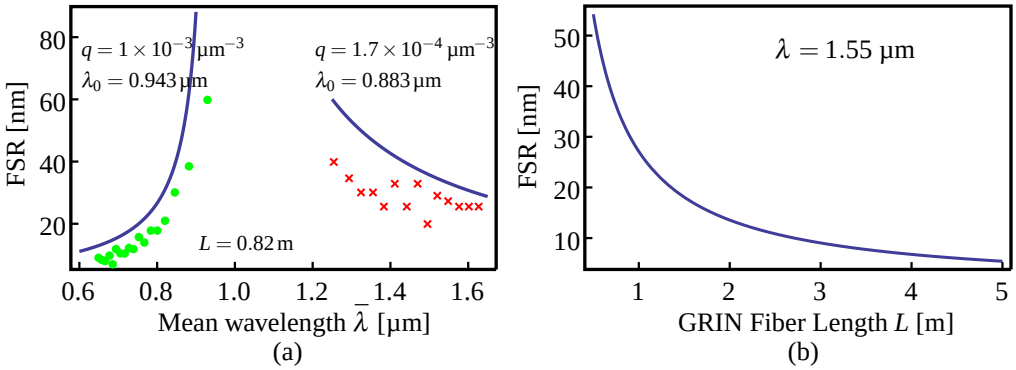

Fig. 3. (a) Free Spectral Range (FSR) as a function of $\bar{\lambda}$ for a constant length. Marks represent experimental values when using Newport FS-V (green dots) and Corning SMF-28 (red crosses) as input single-mode fibers. Further experimental details as explained in Sec. 5. (b) FSR as a function of the multimode fiber's length L for a fixed wavelength. Both graphs are for a conventional SMS sensor while the solid blue line represent an analytical approximation as explained for Eq. (2).

3. The effect of tapering a GRIN fiber

The core of a conventional GRIN fiber has a parabolic refractive index distribution given by the following expression,

$$n(r) = n_0 \left(1 - A_g^2 r^2\right), \qquad r < a$$

where n_0 is the refractive index at the symmetry axis z of the fiber, r is the radial distance for a cylindrical coordinate system, $A_g \equiv a/\sqrt{2\Delta}$ is defined as the specific core radius as in [12], a and Δ are the core radius and the profile height parameter of the fiber, respectively.

By using the parabolic-shaped profile $n(r)$ defined above, the paraxial ray equation can be transformed into an ordinary second order differential equation [13],

$$\frac{d^2 r}{dz^2} + \frac{2r\Delta}{a^2} = 0,$$

#221963 - $15.00 USD Received 29 Aug 2014; revised 10 Nov 2014; accepted 10 Nov 2014; published 1 Dec 2014

valid only for meridional rays. The solution of this equation is given by,

$$r(z) = C_1 \cos(z/A_g) + C_2 \sin(z/A_g), \tag{3}$$

showing how $r(z)$ is a sinusoidal equation with period,

$$T = 2\pi A_g\,. \tag{4}$$

Here it is worth to notice that in Eq. (4), the period is proportional with the core radius.

The constants C_1 and C_2 at Eq. (3) are obtained by taking into account the initial conditions $r(0) = r_0$ and $dr/dz = \gamma_0$, where γ_0 is the input ray angle. In this way the ABCD matrix for a GRIN fiber is obtained [12–14], making possible to predict the position for an input ray (r_0, γ_0) after propagating a distance z,

$$\begin{pmatrix} r \\ \gamma \end{pmatrix} = \begin{pmatrix} \sin(z/A_g) & A_g \cos(z/A_g) \\ -\dfrac{1}{A_g}\cos(z/A_g) & \sin(z/A_g) \end{pmatrix} \begin{pmatrix} r_0 \\ \gamma_0 \end{pmatrix}. \tag{5}$$

As shown by the dashed lines in Fig. 4(a), a GRIN fiber with $A_g = 200\,\mu$m exhibits sinusoidal ray trajectories for different input angles γ_0 in the same way as in [12].

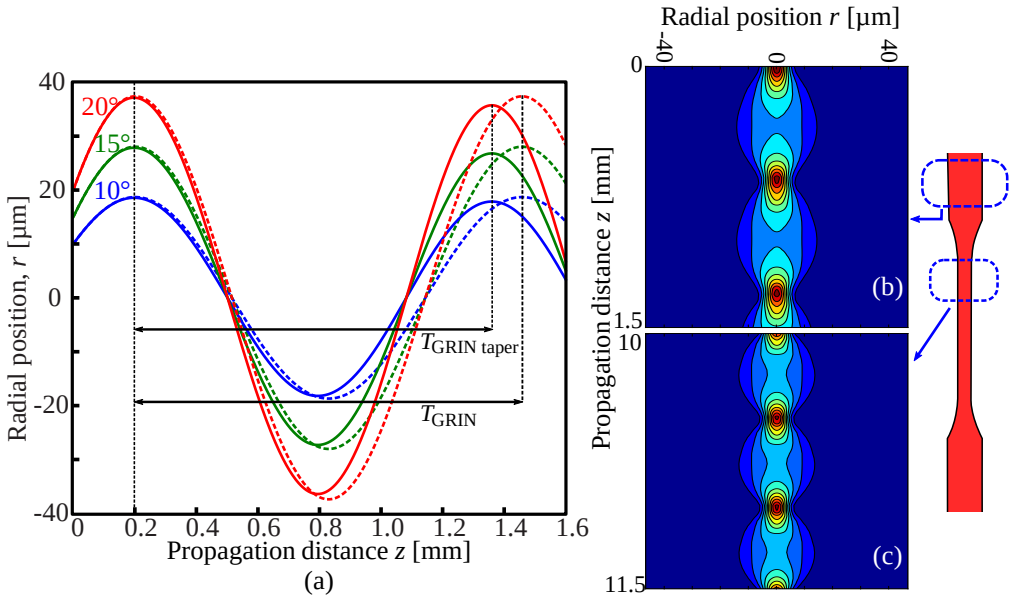

Fig. 4. (a) Ray trajectories for a GRIN fiber using different input angles. Dashed lines represent an homogeneous GRIN fiber with core radius $a_0 = 40\,\mu$m and $A_g = 200\,\mu$m, as in [12]. Solid lines represent the same GRIN fiber but with an exponentially decaying taper profile. The black arrows show the different periods for rays propagating on the tapered and untapered versions of the GRIN fiber. (b and c) Color-coded electric field amplitude for 1.5 mm long slices of a tapered GRIN fiber simulated using RSoft's Beamprop software. Plot (b) is for the homogeneous region, while (c) is for the tapered region of the taper as illustrated by the scheme at right. By choosing the appropriate fiber parameters and the same taper profile, similar results were obtained in comparison with the ray trajectories at left.

#221963 - $15.00 USD Received 29 Aug 2014; revised 10 Nov 2014; accepted 10 Nov 2014; published 1 Dec 2014

While this is considerably accurate for a standard GRIN fiber, it is not for a tapered GRIN fiber where the beam is affected by the proximity of the cladding. However, for a slowly-varying taper profile the effect of varying the fiber diameter can be visualized by defining the core radius as a function of the axial coordinate in such a way that $a(z)$ represents a taper profile function [15]. As shown by the solid lines in Fig. 4(a), the period of the rays trajectories will decrease with the propagation distance for a GRIN fiber with an exponentially decaying taper profile $a(z) = a_0 e^{-i\alpha z}$, with $\alpha \approx 5 \times 10^{-5}\,\mathrm{m}^{-1}$. As shown, black arrows exhibit the difference between the periods for the GRIN fiber (tapered and untapered) after propagating more than 1 mm. Being this one noticeably shorter than the homogeneous fiber, as it is the expected result predicted by Eq. (4).

As a further demonstration, similar numerical results were obtained by modeling a tapered GRIN fiber using a commercially available Beam Propagation Method: RSoft's BeamProp version 2013-12-2. In Fig. 4(b and c), the color scale of the contour maps represent the field amplitude for two different slices of a tapered GRIN fiber with $a_0 = 40\,\mu\mathrm{m}$ and $\Delta = 2\%$. As expected, down-taper the period of the sinusoidal beam waist decreases in the same fashion as the ray optics analysis results. Note also that the inverse effect also occurs up-taper: the period stretches as the diameter increases in the same fashion as in Eq. (4).

4. Sensing characteristics of an SMS sensor with a tapered GRIN fiber

In order to evaluate the sensitivity of this device to external refractive index ($\Delta\lambda/\Delta n$), it becomes necessary to understand the nature of the output intensity peaks in an SMS sensor. The phase difference ($\Delta\phi$) of the two lower order modes can be related to a perturbation parameter, here the external refractive index (Δn), and written as,

$$\Delta\phi = \frac{\partial\phi}{\partial\lambda}\Delta\lambda + \frac{\partial\phi}{\partial n}\Delta n\,. \tag{6}$$

By equating $\Delta\lambda/\Delta n$,

$$\frac{\Delta\lambda}{\Delta n} = \left(\frac{\Delta\phi}{\Delta n} - \frac{\partial\phi}{\partial n}\right)\left(\frac{\partial\phi}{\partial\lambda}\right)^{-1} \tag{7}$$

it can be seen that the external refractive index sensitivity $\Delta\lambda/\Delta n$ will be maximum when the phase difference approaches a critical point, $\partial\phi/\partial\lambda \to 0$ at a critical wavelength λ_0.

Unfortunately, as shown by the blue rhombuses in Fig. 5, the critical wavelength for a GRIN fiber at its nominal size is found at $\lambda_0 \approx 0.925\,\mu\mathrm{m}$. That is, away from the telecom window ($\lambda \sim 1.55\,\mu\mathrm{m}$) where one can take advantage of the multiple light sources, equipment and low-loss fibers commercially available at these wavelengths. While observing the difference between the propagation constants β_1 and β_2 for the two lower order modes LP_{01} and LP_{02} as a function of λ, we saw the critical wavelength (minimum) decreasing as the fiber was tapered down to waists ranging from 125 to 62.5 µm. The latter made the previous situation worse, since the maximum sensitivity point was more distant of the telecom window as the taper waist decreased. Fortunately, by further reducing the outer diameter, a maximum appeared when the taper waist was around 20 µm as shown by the red dots in Fig. 5. Therefore, the critical point for maximum sensitivity can be tuned by selecting the appropriate taper waist $D_w = 15\,\mu\mathrm{m}$ as shown by black crosses for a critical wavelength close to $\lambda \approx 1.6\,\mu\mathrm{m}$.

After varying the taper waist, we studied the effect of varying the outer refractive index. The numerical results showed that this type of sensors are sensitive to external refractive index variations only when the taper waist is under 20 µm. Figure 6(a) shows curves representing $\beta_1 - \beta_2$ for different outer refractive indexes as shown in the legend box. A minimum phase difference can be observed when $D_w = 20\,\mu\mathrm{m}$ and $\lambda > 2.0\,\mu\mathrm{m}$, while a considerable influence

#221963 - $15.00 USD Received 29 Aug 2014; revised 10 Nov 2014; accepted 10 Nov 2014; published 1 Dec 2014

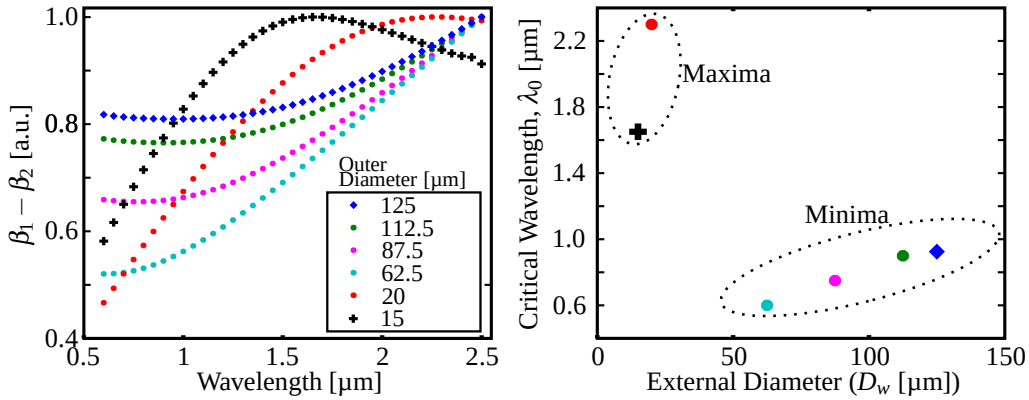

Fig. 5. (a) Dependence of $\beta_1 - \beta_2$ as a function of wavelength for a tapered GRIN fiber (normalized data). (b) Critical wavelength for different outer diameters. For both figures, different colors represent different cladding diameters for the tapered fiber as shown in the legend box. All the results are for an outer refractive index $n = 1.39$ RIU obtained using a Finite Element software [10].

of the external refractive index was observed for $D_w = 15\,\mu$m and $\lambda > 1.6\,\mu$m. A zoom over the critical point is shown on Fig. 6(b) for $D_w = 15\,\mu$m. On Fig. 6(c), critical wavelengths are plotted as function of the outer refractive index exhibiting an almost linear behavior. Up to our knowledge, previous SMS sensors using GRIN fibers were not sensitive to external refractive index variations nor had their maximum sensitivity spectral region tuned.

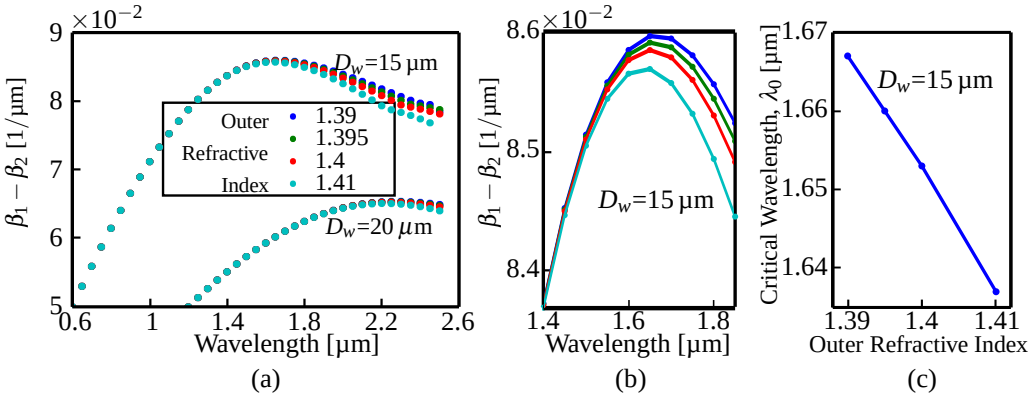

Fig. 6. (a) Propagation constant difference for the two lower-order modes LP_{01} and LP_{02} at the tapered GRIN fiber as a function of wavelength. It can be seen that an SMS sensor will only be sensitive to external refractive index variations (different colored disks) when using tapers thinner than $D_w \leqslant 20\,\mu$m. (b) Zoom of the previous plot around the critical wavelength for $D_w = 15\,\mu$m. A small shift of the maximum toward lower wavelengths can be observed when the external refractive index increases. (c) An almost linear behavior is observed for the critical wavelengths as the outer refractive index varies. All results obtained using a Finite Element software [10].

#221963 - $15.00 USD Received 29 Aug 2014; revised 10 Nov 2014; accepted 10 Nov 2014; published 1 Dec 2014

5. Sensing results

To construct the proposed SMS tapered sensor, a traveling burner tapering system [15] was used for the fabrication of the GRIN fiber tapers. Each transition region was approximately 30 mm long tapered with an exponentially decaying profile. The same GRIN fiber as in Sec. 2, a GIF625 from Thorlabs, was used as the multimode fiber for the following experimental results. The assumption of a perfect alignment exposed in Sec. 1, is not an impediment for the implementation of the proposed experiment. That is because the fractional modal power of modes LP_{01} and LP_{02} will represent more than the 60% of the total power for misalignments under 5 µm and $\lambda > 1.3\,\mu m$ as shown in Fig. 2. An splicer machine automatically adjusted the splicing parameters –such as the electrodes position, relative fiber alignment and splicing power– reducing the fiber misalignments below this limit.

In order to evaluate the performance of a tapered SMS sensor as an external refractive index sensor, the sample was immersed in a refractive index matching liquid initially at $T = 20\,^{\circ}C$ and fixed straight while being careful not to stretch the taper. Later, the liquid was heated by a hot plate and temperature was controlled by a thermocouple. Temperature change ΔT determined the external refractive index change Δn by the expression,

$$\Delta n = (dn_0/dT)\Delta T\,, \tag{8}$$

where $n_0 = 1.39$ is the external refractive index at $T = 25\,^{\circ}C$ and $dn_0/dT = -3.44 \times 10^{-4}$ is the thermo-optic coefficient for the AAA series of the Cargille refractive index liquids used during all the experiments. In this way it was possible to control the variation of the external refractive index by controlling the change in temperature. This allowed us to use the same liquid for all measures. Since the measurements were done in a temperature range $0 < \Delta T < 6\,^{\circ}C$, the effect of the temperature over the fiber may be negligible as shown in [4] for a GRIN SMS used as a temperature sensor.

As stated before, the output spectrum for a non-tapered SMS sensors is a mode interference pattern composed of several peaks as shown by the red curve in Fig. 7(a). By choosing a peak and measuring the shift $\Delta\lambda$ caused by the change of temperature or external refractive index, it is possible to determine the sensitivity of this device ($\Delta\lambda/\Delta n$ or $\Delta\lambda/\Delta T$) as in Eq. (7). Since the spectral resolution of the SMS sensor depends inversely on the FSR, it is critical to design an SMS sensor with a FSR as low as possible. On the other hand, it is important to note that this also reduces the dynamic range of the measurement. Also, as shown in Fig. 3(b), a GRIN fiber longer than 5 m is necessary to obtain a FSR under 5 nm. Nevertheless, by tapering the GRIN fiber of the SMS sensor as in Fig. 1(b), the period of the modulated beam is spatially compressed as explained above. For that reason, the taper acts as a substitute of a much longer multimode fiber. As an example, as shown in Fig. 7(a), the output spectrum of a 3 m long SMS sensor exhibit a large FSR whereas a tapered SMS sensor whose total length –tapered and untapered sections– is shorter than 1 m exhibits a considerable lower FSR in the same optical window. That is, an untapered SMS is more than three times longer than the tapered SMS sensor here proposed. Inset shows numerical results for the phase difference as a function of wavelength, a similar behavior as in the experimental results can be observed. The shift of the peak $\Delta\lambda$ as a function of the change in the external refractive index Δn is shown for the experimental results in Fig. 7(b). A linear behavior is observed through all the studied range and its slope represents a sensitivity of $\Delta\lambda/\Delta n = 3842\,nm/RIU$, which is equivalent to a temperature response $\Delta\lambda/\Delta T = 1.32\,nm\,^{\circ}C^{-1}$. Inset shows the spectra used to make the measurements in Fig. 7(b), where the chosen set of peaks were those closer to $\lambda = 1.54\,\mu m$.

#221963 - $15.00 USD Received 29 Aug 2014; revised 10 Nov 2014; accepted 10 Nov 2014; published 1 Dec 2014

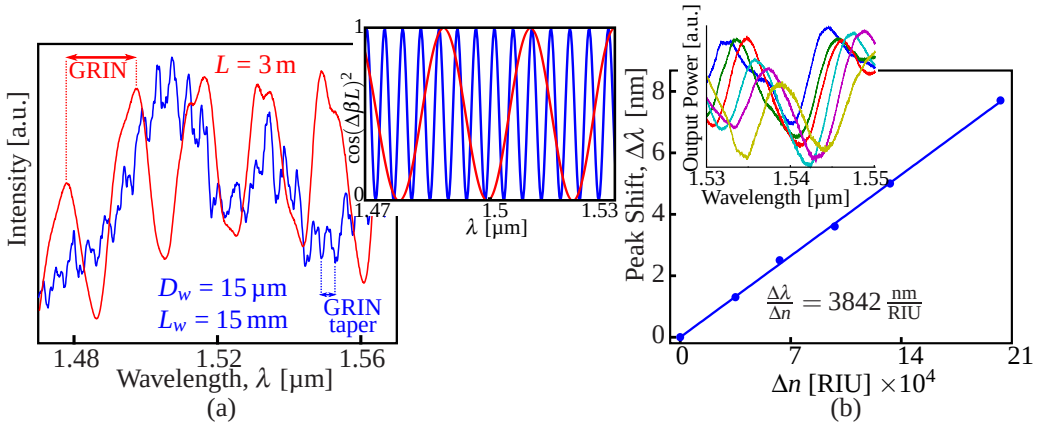

Fig. 7. (a) Comparison between the output intensity spectrum for a conventional SMS sensor (red) made with a 3 m long GRIN fiber and a tapered GRIN fiber (blue) whose total length is shorter than 1 m (a uniform waist length $L_w = 15$ mm, plus two transition regions of ≈ 30 mm long). Inset shows the numerical results for $\cos(\Delta\beta L)^2$ as a function of wavelength. (b) Peak shift as a function of the outer refractive index difference. Inset shows the spectra used to obtain a sensitivity of 3842 nm/RIU. For all graphs, the taper transition region of the GRIN fiber has an exponential form similar as in Fig. 1(b).

6. Conclusion

By tapering a GRIN fiber –spliced in-between two single-mode fibers– we have constructed a compact, robust and accurate outer refractive index optical SMS microsensor. In comparison with previous results, in [4] a highly accurate strain and temperature SMS sensor is presented using a GRIN fiber as the multimode waveguide. Here the MMF is not tapered and, in consequence, it is not possible to get the most out of the overlap between the evanescent field and the external medium to be sensitive to external refractive index changes. On the other hand, in [7] a tapered step-index multimode fiber sandwiched between two SMFs exhibits a wide dynamic range as a refractometer. A similar proposal was made in [5], where authors report a maximum sensitivity of 2946 nm/RIU. These proposals are more difficult to construct since coupling between a step-index MMF and an SMF depend on the self-imaging distance, therefore high precision is necessary for cutting and splicing the MMF. Also, measurements in [7] and [5] are based in the transmission loss as a function of the external refractive index. This makes necessary to make highly accurate measurements of the transmission loss P in order to precisely determine the refractive index change.

After constructing for the first time (up to our knowledge) a tapered GRIN SMS microsensor, we attained a maximum sensitivity of 3842 nm/RIU. In addition, two different benefits upgrade the sensitivity of the SMS sensors: first, the critical wavelength –which determines the maximum sensitivity region– can be tuned in a great extension. Here we have shown how to tune the maximum sensitivity wavelength towards the optical telecom window. This make possible to use commercially available light sources as well as improve the sensitivity at an arbitrary wavelength for a specific application (i.e. biological sensors). Second, despite the resolution of the SMS sensor depends on the length of the multimode fiber, we found a way to reduce the dimensions of the SMS sensor by an order of magnitude while attaining high resolution. These two improvements in conjunction signifies a considerable upgrade for the proposed SMS sensor, making it a more compact and precise measuring device.

#221963 - $15.00 USD Received 29 Aug 2014; revised 10 Nov 2014; accepted 10 Nov 2014; published 1 Dec 2014

Acknowledgments

F. Beltrán-Mejía gratefully acknowledges financial support from São Paulo Research Foundation, FAPESP (grant 2011/01524-8).

#221963 - $15.00 USD Received 29 Aug 2014; revised 10 Nov 2014; accepted 10 Nov 2014; published 1 Dec 2014